Size-controllable ZnS nanospheres: synthesis and enhanced photocatalytic activity

CHAO JIAO, WEI-QING HUANG*, GUI-FANG HUANG*, ZHI-DAN SU[a], MING-GANG XIA[a], ZHENG-MEI YANG, ZHUO WAN, QING-LIN ZHANG

Department of Applied Physics, Key Laboratory for Micro-Nano Physics and Technology of Hunan Province, Hunan University, Changsha 410082, China

[a]MOE Key Laboratory for Nonequilibrium Synthesis and Modulation of Condensed Matter, Center on Experimental Physics, School of Science, Xi'an Jiaotong University, 710049 China

Increasing specific surface area and high-index facets of photocatalyst is vital to enhance photocatalytic properties. We report here that well-dispersed and uniform ZnS nanospheres with controllable size have been synthesized via a low-cost and simple chemical bath deposition. It is interesting that both the size and high-index facets of ZnS nanospheres can be modulated only by tuning bath temperature. The porous ZnS nanospheres prepared at 95℃ possess the highest catalytic activity due to the larger specific area, as well as easier separation of electron-hole pairs by photoexcitation. The results indicate that the porous ZnS nanospheres are promising candidate materials for photocatalysts. Our results shed new light on the preparation of highly efficient semiconductor photocatalysts used in environmental remediation applications.

(Received October 28, 2013; accepted July 10, 2014)

Keywords: ZnS, photocatalytic activity, Specific surface area, Chemical bath deposition

1. Introduction

Semiconductor photocatalysis has been considered as an efficient and environmentally friendly method for environmental remediation and new clean energy production [1-7] since it can decompose various organic compounds or photocatalytic split water into H_2 and O_2 with light irradiation. A large amount of new compounds and materials for photocatalysis has been proposed in the recent years. As an important II–VI compound semiconductor photocatalyst [8-11], ZnS nanomaterials show efficient catalytic activity and application prospect in the photocatalytic degradation of toxic organic pollutants [6, 12]. To date, however, industrial treatment of pollutants by photocatalytic oxidation with ZnS is uncommon because of the low photodegradation efficiency. Therefore it is highly desirable to improve the photocatalytic properties of ZnS by using economical methods.

It is generally accepted that the photocatalytic reaction occurs primarily at the interface where the pollutants contact with the active surface of the photocatalyst [13-16]. Therefore, the photocatalytic properties of photocatalysts mainly depend on the specific surface area and surface atomic rearrangement and coordination [17, 18], which modulate the crystal facets in different orientations. Numerous researches have been demonstrated that the photocatalyst's activity significantly varies with specific surface area and exposed crystal facets. For example, elongated truncated tetragonal bipyramid (ETTB) anatase [19] and terminal polar of ZnO with highly energy facets exhibit highly photocatalytic activity [20]. These results reveal that designing photocatalysts with large specific area and/or highly energy facets exposed is the promising avenue to improve their photocatalytic properties [21-23]. It is, however, rather challenging to synthesize ZnS with high-index facets because of their high surface energy. As is known, crystal growth rates in the direction perpendicular to a high-index plane are usually much faster than those along the normal direction of a low-index plane, so high-index planes are rapidly eliminated during particle formation based on minimization of surface energy.

In this work, chemical bath deposition (CBD) is chosen to synthesize ZnS nanospheres because it is an attractive method performed under low temperature and ambient pressure, making it an easy and inexpensive technique. It is interesting that only by raising bath temperature to increase the speed of nucleation and growth rate, ZnS nanospheres with larger specific area and more high-index facets can be obtained. The ZnS nanospheres prepared at 95℃ exhibit superior photocatalytic activity, providing a feasible and practical method to prepare photocatalysts with high activity.

2. Experiment

ZnS nanospheres were synthesized with following process. Solution A was fabricated by sufficiently dissolving 11.7 mmol tri-sodium citrate and 8.5 mmol zinc sulfate in 343 mL deionized water. Solution B was prepared by dissolving 49.5 m mol thiourea in 50.0 mL deionized water. The pH of solution A was adjusted to 8.5 using ammonium hydroxide. Solution A was heated to 65 ℃, 75 ℃, 85 ℃ and 95 ℃ in thermostatic water

bath respectively, then solution B was mixed with A. The mixture was stirred continuously for 3 h. The precipitate was centrifuged and washed several times with deionized water and absolute ethanol, and was then dried in vacuum oven at 45 ℃ for 12 h.

The structures and morphologies of the products were characterized by X-ray diffraction (XRD, Siemens D-5000 diffractometer with Cu Kα irradiation), micro-Raman spectroscopy (Horiba LabRAM HR800 apparatus) with He laser beam at 325 nm line, scanning electron microscope (SEM, Hitachi S-4800), transmission electron microscope (TEM, FEI Tecai F20), and BET(Brunauer, Emmett and Teller) measurement. The optical absorption spectra of the samples dispersed in ethanol were recorded using a double beam UV-VIS spectrophotometer (TU-1901). The photo-induced charge separation in the samples was demonstrated by surface photovoltaic voltage (SPV) measurement.

The photocatalytic activity of ZnS nanospheres was evaluated by photodegradation of aqueous solution of methylene blue (MB) under the irradiation of a 300 W UV lamp. The catalytic experiments were implemented with 80 mL 3.13×10^{-5} M MB solution and 10 mg ZnS sample. The suspension was magnetically stirred in dark for 15 mins to reach the adsorption equilibrium before illumination. During irradiation, the samples were taken out at regular time intervals and centrifuged to wipe off the catalysts. The absorption spectra of the solution were determined using UV-VIS spectrophotometer.

3. Results and discussion

Controlled synthesis of cubic ZnS structures with unique surface atomic rearrangements is successfully achieved by CBD. Detailed analyses on the synthesized samples are carried out using XRD analysis. Fig. 1 displays the XRD patterns for the prepared ZnS nanospheres. The diffraction peaks at about 29.18º (111), 48.72º (220), and 58.04º (311) can be well indexed to the cubic structure of ZnS (JCPDS NO. 79-0043) [24], with the average crystallite sizes of 2.62, 2.79, 2.84 nm respectively, which are calculated using the Debye-Scherrer formula, as the temperature rises from 75℃ to 95℃. No characteristic peaks ascribing to other phases are observed, which confirms that the prepared nanospheres possess high purity of ZnS cubic phase. However, the obvious changes in the intensity ratios for specific peaks are worth noticing. The intensity ratios of {220}/{111} and {311}/{111} for ZnS prepared at 95℃ are 0.89 and 0.82 respectively, which are much higher than those (0.54 and 0.45) of ZnS prepared at 75℃. The enhancement of high-index facets are similar to those reports on TiO_2 and Ag_3PO_4, which would lead to higher photocatalytic activity [25]. The percentage of crystallographic facet relies on the relative stability of each surface during crystal growth. At lower temperature, ZnS nucleation and growth rate are relatively low, the crystal growth process follows the principle of surface energy minimization and leads to the minimum of highly active facets. When the crystal nucleation and growth rate are fast enough, on the contrary, high-index facets of ZnS will be increased because atomic arrangements don't have enough time to follow the principle of surface energy minimization before new atoms reach the crystal surface at higher temperature. As a consequence, the percentage of high-index facets of ZnS nanospheres increases as the bath temperature rises, which provides the possibility to enhance the photocatalytic activity.

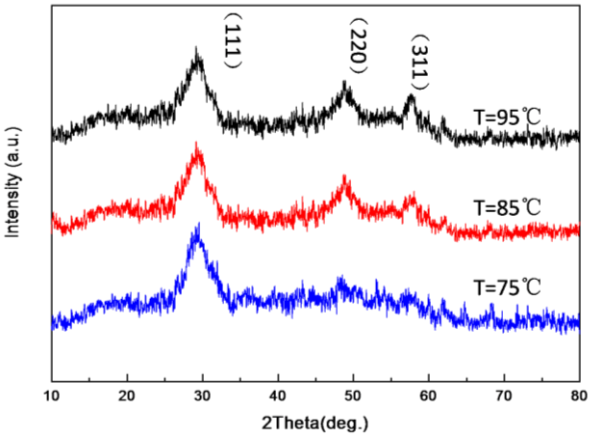

Fig. 1. XRD patterns of ZnS nanospheres.

Raman spectroscopy is also used to examine the structure of ZnS nanospheres. Fig. 2 shows that all samples exhibit two intense peaks centered at 326.53 and 491.83cm^{-1} and two weak peaks centered at 175.51 and 653.06 cm^{-1}, respectively. The peaks at 326.53 and 653.06 cm^{-1} are associated to the first-order longitudinal optical phonon (1LO) and second (2LO) vibration mode of ZnS [26, 27]. The peak at 175.51 cm^{-1} can be allotted as transverse acoustic phonon (TA) vibration mode of ZnS [27]. The peak at 491.83 cm^{-1} is typical Raman shift of silicon substrate. The Raman spectra further confirm the cubic structure of ZnS. It is well known that intensity of Raman signals is proportional to scattering area. The increasing of Raman intensity with temperature increasing from 75℃ to 95℃ suggests the size variation of ZnS nanospheres.

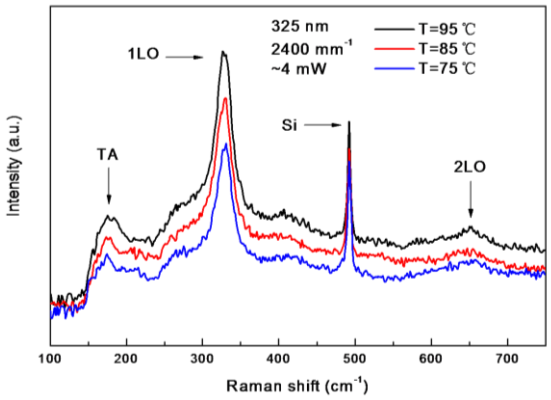

Fig. 2. Raman spectra of different samples with 325 nm He laser as the excitation source.

SEM images of the prepared ZnS samples reveal that all the ZnS samples are consisted of well-dispersed nanospheres with uniform size and well-defined spherical morphology, as shown in Figs. 3 (a-d). The average size of ZnS nanospheres are respectively 55, 111.9, 135.6 and 179.7 nm with the temperature varying from 65℃ to 95℃, demonstrating that the sphere size can be easily controlled only by tuning the temperature. From the TEM micrographs in Figs. 3 (e) and (f), one can see that these spheres are fairly rough and porous, illustrating that the spheres are composed by smaller particles with the diameter about several nm, which is quite consistent with XRD analysis. The rough surface means that the ZnS samples may provide large specific surface area and thus more reactive sites for adsorbing pollutants, which is benefit to the photocatalytic reaction. A set of concentric rings observed from the selected area diffraction (SAED) patterns (the inset in Fig. 3(f)) shows that the prepared nanospheres are polycrystalline and the three concentric rings can be corresponded to (111), (220), and (311) planes of cubic ZnS. The BET measurement is used to survey surface area of ZnS nanosphere samples. The specific surface areas of ZnS nanospheres are 43.1173 m^2/g (T=95℃) and 12.5350 m^2/g (T=75℃) as determined by BET. The specific surface area of the former is more than three times than the latter, which may provide more reactive sites for adsorbing pollutants and the photocatalytic reaction.

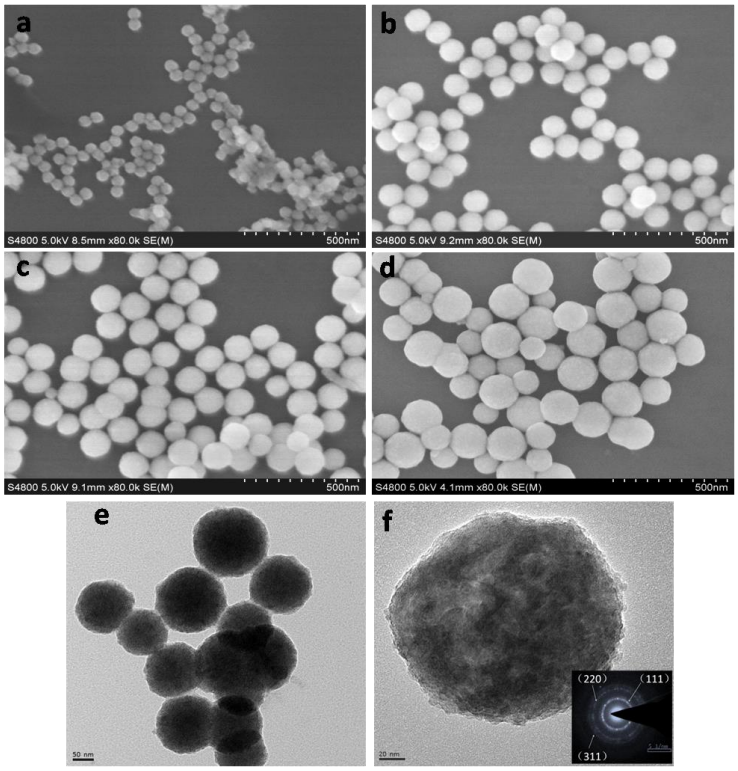

Fig. 3. SEM image of porous ZnS nanospheres synthesized at (a) T=65 ℃; (b) T=75 ℃; (c) T=85 ℃; (d) T=95 ℃. (e, f) low and high magnification TEM image of the sample synthesized at T=95 ℃. The inset in (f) shows the corresponding SAED pattern.

SPV technique is a well-established contactless and non-destructive technique for semiconductor characterization that relies on analyzing illumination-induced changes in the surface voltage [28], and it is proved to be one of the most effective methods to reflect the separation and recombination situation of photogenerated charges to a certain extent. Thus SPV measurements are carried out to explore the photovoltaic properties of ZnS samples. Fig. 4 shows SPV response of the as-produced ZnS nanospheres obtained from different bath temperatures. It is clear that SPV response for all samples features a peak located at about 330 nm, which corresponds to the UV–vis absorption band at 325 nm (the inset in Fig. 4) and can be attributed to the electron transitions from valence band to conduction band (band-to-band transitions) of ZnS. The SPV response intensity increases with the bath temperature increasing from 65℃ to 95℃. The reason for this is mainly the difference in particle sizes [29]. The stronger SPV response is caused by more photo-generated charge carriers transfer to the surface before their recombination, indicating that more high-index facets of ZnS could be more favorable to separation of photo-generated electron-hole pairs. This is also true for UV–vis absorption: the absorption of ZnS nanospheres enhances with the temperature increase (see the inset in Fig. 4). So it can be speculated that the photocatalytic ability of ZnS prepared at 95℃ may be best.

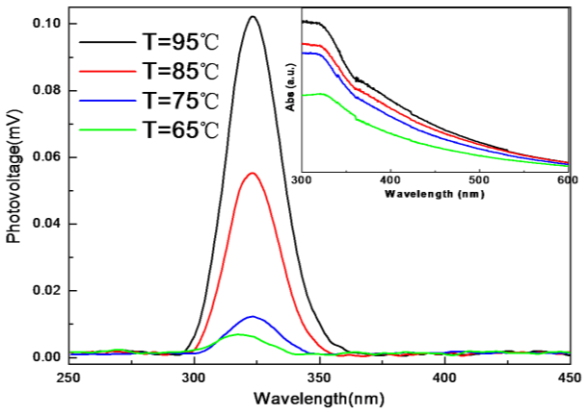

Fig. 4. SPV spectra of as-prepared ZnS nanospheres at T=65 ℃; T=75 ℃; T=85 ℃; T=95 ℃. The inset is optical absorption spectra of the ZnS nanospheres.

It has been proved that ZnS is an efficient photocatalyst for degradation of water pollutants and reduction of toxic metal ions. To explore the potential applicability of the as-prepared ZnS nanospheres, the photocatalytic activity by choosing the degradation of MB solution is investigated at room temperature. The characteristic absorption of MB at about 664 nm is chosen as the monitored parameter for the photo-degradation process. The continuous decrease in the intensity of absorbance peaks (Fig. 5 (a)), corresponding to a series of color changes sequence (inset of Fig. 5 (a)), indicates the continuous decrease in concentration of an aqueous solution of MB in presence of ZnS nanospheres (T=95℃) under UV light irradiation as the exposure time increases. It can be seen that the absorption peaks almost disappear and the dark blue color of the beginning solution fades away after irradiation for 18 min. The slight blue-shift of absorption peaks with increase of exposure time could be attributed to a de-ethylated process of MB in a stepwise manner [30]. No new absorption bands emerge in the whole spectrum, which illustrates the complete decomposition of MB. In order to distinguish the photodegradation activity of photocatalysts from the contribution of the decomposition of MB itself, a test of decomposition of MB itself under UV-light irradiation without ZnS photocatalyst was carried out. The decrease in the concentration of MB without photocatalyst as inserted in Fig. 5 (b) is negligible under the same UV-light irradiation for 60 mins, indicating the stabilization of MB.

Fig. 5 (c) illustrates the degradation efficiency of MB with ZnS photocatalyst prepared at different temperature. It is clear that all the samples display efficient photocatalytic activity for MB degradation. As shown in Fig. 3, all the porous nanospheres are consisted of small particles. The unique structure provides large specific surface area and more reactive sites for the photocatalytic reaction and facilitates the transfer of photogenerated electron-hole pairs to the surface/interface, which can inhibit electron-hole recombination and thus enhance the photocatalytic activity. Fig. 5 (c) shows that 97.2% of the MB is photocatalytically degraded after 18 min irradiation for ZnS nanospheres prepared at 95℃. This indicates that the obtained samples have potential application in photocatalytic organic compounds. The kinetic data curves for MB photocatalytic degradation with photocatalyst inserted in Fig. 5(c) show that the relationship between ln (C_0/C_t) (C_0 and C_t are the initial concentration and the concentrations of MB after irradiation t min, respectively) and irradiation time is almost linear, suggesting that the photocatalytic reaction follows the pseudo-first-order kinetics. The photocatalytic rate constant k for MB decomposition with ZnS nanospheres prepared at 95℃ is about 0.0067 min-1, much faster than that with ZnS nanospheres prepared at 65℃ (0.0018 min-1). The results show that ZnS nanospheres prepared at 95℃ possesses the highest catalytic activity, followed by the samples prepared at 85℃, 75℃, and 65℃, respectively. Table 1 lists the photodegradation efficiency of ZnS [31-32]. It can be seen that the porous ZnS prepared in this work can effectively degrade MB with the shortest irradiation time. This indicates that our work provides a simple and economical CBD method to synthesize effective photocatalyst. Since the photoreaction mainly proceeds on the surface of photocatalyst, the photocatalytic activity depends on the co-effects of material morphology, specific surface area, charge-carrier dynamics and light absorption efficiency. As discussed above, ZnS nanospheres prepared at 95℃ have the largest surface area and percentage of high-index facets, which provide more reactive sites at the surface for adsorbing MB and the photocatalytic reaction. Moreover, the separation of electron-hole pairs by photoexcitation is easier in ZnS nanospheres prepared at 95℃. The combined effect of all these factors results in the superior photocatalytic activity of ZnS nanospheres prepared at 95℃.

Table 1. The comparison of degradation efficiency for ZnS with those reported.

Photocatalysts (ZnS/mg)	**Methylene blue (MB/g)**	**Time of Photodegradation (min)**	**Reference**
150	2.5×10^{-3}	40	[31]
180	1.2×10^{-2}	35	[32]
10	8.0×10^{-4}	18	this work

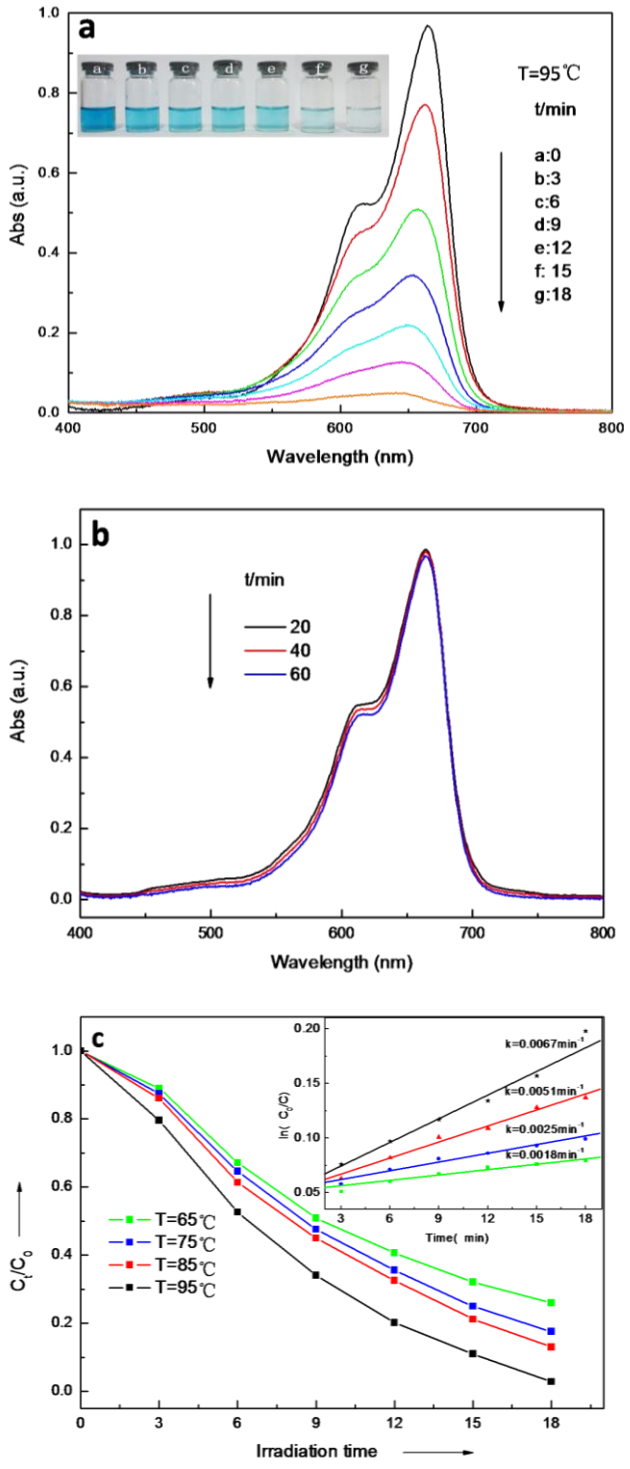

Fig. 5. (a) Absorption spectra of MB solution in the presence of porous ZnS nanospheres under UV light irradiation. The inset is a series of color changes sequence with irradiation times. (b) The decomposition of MB itself under UV-light irradiation. (c) Comparison of photocatalytic activities of different samples for the photodegradation of MB. The inset is the relative kinetic rates.

4. Summary

In summary, well-dispersed and uniform ZnS nanospheres have been prepared by an economical CBD. The ZnS nanospheres are porous since they are the aggregates of small particles. Both the size and high-index facets of ZnS nanospheres increase as the bath temperature rises. The more high-index facets in ZnS nanospheres can be attributed to the rapid nucleation and growth rate at higher temperature. Due to larger specific area, more high-index facets, as well as easier separation of electron-hole pairs by photoexcitation, ZnS nanospheres prepared at 95℃ have the highest catalytic activity. The results indicate that the porous ZnS nanospheres are promising candidate materials for photocatalysts. The method, by regulating the nucleation and growth rate to synthesize crystals with high-index facets, would provide new insight into the preparation of semiconductor photocatalysts with highly efficient activity. It is expected that this simple and economical CBD route can also be extended to the preparation of other UV functional materials and other metal chalcogenides, which makes it useful in the treatment of polluted water. The effective and low-cost method with large scale production has practical applications.

Acknowledgements

This work is supported by Science and Technology Plan Projects of Hunan Province (2013SK3148), the Hunan Provincial Natural Science Foundation of China (Grant No. 12JJ3009). M. X. thank support by the Fundamental Research Funds for Central Universities (Nos. xjj2011001 and 2012jdgz04), and by the Scientific Research Foundation for the Returned Overseas Chinese Scholars, State Education Ministry.

Reference

[1] Z. G. Zou, J. H. Ye, K. Sayama, H. Arakawa, Nature, **414**, (6864), 625 (2001).
[2] Y. Tian, G.-F. Huang, L. J. Tang, M.-G. Xia, W.-Q. Huang, Z.-L. Ma, Materials Letters, **83**, 104 (2012).
[3] G. Gai, X. Dong, L. Wang, X. Pan, X. Chen, Optoelectron. Adv. Mater.-Rapid Comm., **6**(5-6), 568 (2012).
[4] J. S. Hu, L. L. Ren, Y. G. Guo, H. P. Liang, A. M. Cao, L. J. Wan, C. L. Bai, Angewandte Chemie-International Edition, **44**(8), 1269 (2005).
[5] C. W. Lai, S. Sreekantan, Optoelectron. Adv. Mater.-Rapid Comm., **6**(1-2), 82 (2012).
[6] P. Gowthaman, M. Saroja, M. Venkatachalam, J. Deenathayalan, T. S. Senthil, Optoelectron. Adv. Mater.-Rapid Comm., **5**(12), 1307 (2011).
[7] J. S. Hu, L. L. Ren, Y. G. Guo, H. P. Liang, A. M.

Cao, L. J. Wan, C. L. Bai, Angewandte Chemie-International Edition, **44**(8), 1269 (2005).
[8] Y. Chen, G.-F. Huang, W.-Q. Huang, L.-L. Wang, Y. Tian, Z.-L. Ma, Z.-M. Yang, Materials Letters, **75**, 221 (2012).
[9] J. Zhang, J. Yu, Y. Zhang, Q. Li, J. R. Gong, Nano Letters, **11**(11), 4774 (2011).
[10] C. Dagui, H. Feng, R. Guoqiang, L. Dongsong, Z. Meng, W. Yongjing, L. Zhang, Nanoscale, **2**(10), 2062 (2010).
[11] H. C. Ong, R. P. H. Chang, Applied Physics Letters, **79**(22), 3612 (2001).
[12] Z. Jun, L. Shengwei, Y. Jiaguo, M. Jaroniec, Journal of Materials Chemistry, **21**(38), 14655 (2011).
[13] A. Hameed, T. Montini, V. Gombac, P. Fornasiero, Journal of the American Chemical Society, **130**(30), 9658 (2008).
[14] J. Zhang, Q. Xu, Z. Feng, M. Li, C. Li, Angewandte Chemie-International Edition, **47**(9), 1766 (2008).
[15] X. H. Yang, Z. Li, C. Sun, H. G. Yang, C. Li, Chemistry of Materials, **23**(15), 3486 (2011).
[16] F. Long, W.-M. Wang, Z.-k. Cui, L.-Z. Fan, Z.-g. Zou, T.-k. Jia, Chem. Phys. Lett., **462**(1-3), 84 (2008).
[17] F. F. Canova, S. Kawai, C. de Capitani, K.-i. Kan'no, T. Glatzel, B. Such, A. S. Foster, E. Meyer, Physical Review Letters, **110**(20), (2013).
[18] E. S. Jang, J.-H. Won, S.-J. Hwang, Advanced Materials, **18**(24), 3309 (2006).
[19] R. Boppella, K. Anjaneyulu, P. Basak, S. V. Manorama, Journal of Physical Chemistry C, **117**(9), 4597 (2013).
[20] L. Pan, J.-J. Zou, S. Wang, X.-Y. Liu, X. Zhang, L. Wang, Acs Applied Materials & Interfaces, **4**(3), 1650 (2012).
[21] S. Liu, J. Yu, M. Jaroniec, Chemistry of Materials, **23**(18), 4085 (2011).
[22] M. Mlambo, M. J. Moloto, N. Moloto, P. S. Mdluli, Materials Research Bulletin, **48**(6), 2196 (2013).
[23] V. Robles, J. F. Trigo, C. Guilleacuten, J. Herrero, J. Mater. Sci., **48**(11), 3943 (2013).
[24] S. Lee, D. W. Song, D. J. Kim, J. Lee, S. Kim, I. Y. Park, Y. D. Choi, Materials Letters, **58**(3-4), 342 (2004).
[25] Y. Bi, S. Ouyang, N. Umezawa, J. Cao, J. Ye, Journal of the American Chemical Society, **133**(17), 6490 (2011).
[26] W. G. Nilsen, Physical Review, **182**(3), 838 (1969).
[27] J. Serrano, A. Cantarero, M. Cardona, N. Garro, R. Lauck, R. E. Tallman, T. M. Ritter, B. A. Weinstein, Physical Review B, **69**(1), (2004).
[28] Y. Lu, L. Wang, D. Wang, T. Xie, L. Chen, Y. Lin, Materials Chemistry and Physics, **129** (1-2), 281 (2011).
[29] Y. H. Lin, D. J. Wang, Q. D. Zhao, M. Yang, Q. L. Zhang, Journal of Physical Chemistry B, **108**(10), 3202 (2004).
[30] T. Watanabe, T. Takizawa, K. Honda, Journal of Physical Chemistry, (81), 1845 (1977).
[31] X. J. Wang, F. Q. Wan, K. Han, C. X. Chai, K. Jiang, Materials Characterization, (59), 1765 (2008).
[32] S. A. Feng, J. H. Zhao, Z. P. Zhu, New Carbon Materials, **3**(23), 228 (2008).

*Corresponding author: wqhuang@hnu.edu.cn, gfhuang@hnu.edu.cn